https://doi.org/10.5194/angeo-2020-31
Preprint. Discussion started: 2 June 2020

Annales Geophysicae Discussions

Vlasov simulation of electrons in the context of hybrid global models: A Vlasiator approach

Markus Battarbee[1], Thiago Brito[1], Markku Alho[1], Yann Pfau-Kempf[1], Maxime Grandin[1], Urs Ganse[1], Konstantinos Papadakis[1], Andreas Johlander[1], Lucile Turc[1], Maxime Dubart[1], and Minna Palmroth[1,2]

[1]Space research group, Department of Physics, University of Helsinki, Helsinki, Finland
[2]Finnish Meteorological Institute, Helsinki, Finland

Correspondence: Markus Battarbee (markus.battarbee@helsinki.fi)

Abstract. Modern investigations of dynamical space plasma systems such as magnetically complicated topologies within the Earth's magnetosphere make great use of supercomputer models as well as spacecraft observations. Space plasma simulations can be used to investigate energy transfer, acceleration, and plasma flows on both global and local scales. Simulation of global magnetospheric dynamics requires spatial and temporal scales achievable through magnetohydrodynamics or hybrid-kinetic simulations, which approximate electron dynamics as a charge-neutralizing fluid.

We introduce a novel method for Vlasov-simulating electrons in the context of a hybrid-kinetic framework in order to examine the energization processes of magnetospheric electrons. Our extension of the Vlasiator hybrid-Vlasov code utilizes the global simulation dynamics of the hybrid method whilst modelling snapshots of electron dynamics on global spatial scales and temporal scales suitable for electron physics. Our model is shown to be stable both for single-cell and small-scale domains, and the solver successfully models Langmuir waves and Bernstein modes. We simulate a small test-case section of the near-Earth magnetotail plasma sheet region, reproducing a number of electron distribution function features found in spacecraft measurements.

1 Introduction

Physical processes in near-Earth space are dominated by plasma effects such as non-thermal particle distributions, instabilities, plasma waves, shocks, and reconnection. Modern research into space phenomena utilizes both spacecraft measurements and supercomputer simulations, investigating how ions, electrons, and electric and magnetic fields interact in the vicinity of plasma structures. Spacecraft provide point-like observations, limited in their ability to investigate spatial structures, although modern constellation missions can have multiple satellites close by allowing for multipoint analysis to decipher, e.g., current sheet directions (Escoubet et al., 2001; Burch et al., 2016a). Computer simulations on the other hand are limited by spatial resolution, time stepping, and the large difference between ion and electron temporal and spatial scales (see, e.g., Tóth et al., 2017).

Simulations capable of modelling the whole near-Earth geospace have historically used magnetohydrodynamics, neglecting kinetic effects and implementing electrons only as e.g. the Hall term correction to Ohm's law. These models can be run for extended periods of time, but as they model plasma motion as a fluid, they use coarse grids, e.g. $0.25\,R_{\mathrm{E}}$ (Janhunen et al.,

https://doi.org/10.5194/angeo-2020-31
Preprint. Discussion started: 2 June 2020


Annales Geophysicae Discussions

2012) or $0.1\,R_{\rm E}$ (Wang et al., 2020) (where $R_{\rm E}$ is the Earth radius) and cannot model kinetic effects but are sufficient for some global dynamics. Recent advances have allowed global investigations into hybrid-kinetic models, where ions are treated as a kinetic self-consistent species and electrons are a charge-neutralizing fluid. Successful approaches include hybrid-Vlasov models (Palmroth et al., 2018) and particle-in-cell-codes (e.g. Lin and Wang, 2005; Sibeck et al., 2008; Omidi et al., 2009; Karimabadi et al., 2014). Kinetic investigation run times rarely exceed one hour or hundreds to a few thousand ion gyroperiods. The simulation spatial resolution is chosen to be relevant to the scales of investigation, with the most usual metric being the ion inertial length d_i. The simulation domain must encompass the necessary global dynamics with sufficient space to manage boundary effects.

In order to understand electron physics, kinetic modelling of electrons has been investigated by a number of methods such as full-PIC (ions and electrons as interacting particles, e.g., Hesse et al. 2005), full-Vlasov (ions and electrons as interacting distribution functions, e.g., Umeda et al. 2009; Schmitz and Grauer 2006; Pezzi et al. 2019), hybrid-PIC-electrons (dynamic electron particles, ions as a static background, e.g., Lapenta et al. 2007) and hybrid-Vlasov-electrons (dynamic electron distribution function with ions as a static background, e.g., Nunn 2005). In fully kinetic numerical investigations, the standard approach is to alter the ion-to-electron mass ratio of ~ 1836 to, e.g., 50 (Hesse et al., 2005) or 25 (Wilson et al., 2016) in order to achieve interesting dynamics with available computational resources. Resolving waves and kinetic electron instabilities to prevent simulation self-heating requires the spatial resolution to encompass the Debye length λ_D (Birdsall and Langdon, 2005) and the time stepping must resolve the electron plasma oscillation $\omega_{\rm pe}$. This can, however, be bypassed via semi-implicit or implicit solver methods, at the cost of loss of some electron physics. Effects such as the Dungey cycle (Dungey, 1961), involving the whole magnetosphere, are unachievable with traditional kinetic electron approaches. Full-PIC approaches have, however, been applied to investigations of, e.g., Harris-sheet (Harris, 1962; Lapenta et al., 2015; Daughton et al., 2011) or asymmetric reconnection (Hesse et al., 2016). Pritchett (2000) presents a historical review of magnetospheric PIC simulations and anticipates the development of more realistic, global 3-D magnetosphere models with increasing computational resources.

More recent simulation studies of electron physics in the magnetosphere have focused on local regions, such as modelling of electron diffusion regions (EDRs) and extracting resultant electron velocity distribution functions (eVDFs), such as the PIC simulations by Bessho et al. (2014, 2016) and Hesse et al. (2016). Liu et al. (2013) investigated the small-scale three-dimensional structure of EDRs with a realistic proton-electron mass ratio with a small configuration, and extended to a larger local 3-D configuration with a reduced proton-electron mass ratio. These simulations are always local with prescribed driving. A more global approach, MHD-EPIC, is presented by Daldorff et al. (2014), with a two-way coupling of a global, 2-D Hall MHD magnetosphere model and local implicit PIC model at regions of interest, with a proton-electron mass ratio of 25. Notably, these PIC regions handled by implicit solvers do not resolve the Debye length. MHD-EPIC has since been employed to study the magnetosphere of Ganymede in 3-D with large embedded PIC domains by Tóth et al. (2016); Zhou et al. (2019).

An example of small-scale global, electromagnetic implicit PIC modelling for a weak comet has been performed by Deca et al. (2017, 2019) with a reduced proton-electron mass ratio of 100, and local simulations for a lunar minimagnetosphere (Deca et al., 2015) with a reduced proton-electron mass ratio of 256.

https://doi.org/10.5194/angeo-2020-31
Preprint. Discussion started: 2 June 2020


Annales Geophysicae Discussions Open Access EGU

Ricci et al. (2002) discuss the effect of the ratio between the proton mass m_p and the electron mass m_e as a part of the GEM challenge, concluding that reconnection rates are well captured by smaller mass ratios of $m_\mathrm{p}/m_\mathrm{e} = 180$, although with modified electron kinetics. Lapenta et al. (2010) discusses modifications to electron microphysics at reconnection sites in more detail in relation to proton-electron mass ratios of 64, 256, and 1836 using an implicit PIC model.

Another approach compared to PIC simulations is to represent particle velocity distributions with moments. For example, Huang et al. (2019) have developed a local six-moment multi-fluid full-Maxwell model. For their six-moment code, Huang et al. note that they do not capture reconnection.

Several processes that occur in the magnetosphere that depend on electron behavior are still poorly understood. Recently, missions such as Magnetospheric MultiScale (MMS; Burch et al., 2016a) have enabled plasma measurements that are able to better resolve electron-scale physical processes. MMS in particular has provided data to many publications on magnetic reconnection (e.g., Burch and Phan, 2016; Phan et al., 2018; Huang et al., 2018; Hoilijoki et al., 2019a; Fargette et al., 2020), the most popular topic of electron physics investigations. Another topic of focus is electron-driven waves, such as have been observed recently in different regions of the magnetosphere (e.g., Cattell et al., 2005; Ergun et al., 2016). They have been characterized as whistler mode waves, electrostatic solitary waves and lower hybrid waves among other types. These waves interact strongly with electrons, causing effects such as heating, temperature anisotropy and particle energization.

This paper introduces an alternative, novel method for simulating electron distribution function physics in the context of global ion-determined fields. The aim is to investigate how much of the global electron physics and distribution functions can be understood by utilising ion-generated field as modelled by hybrid-kinetic codes, as opposed to a numerically unfeasible global full-kinetic approach. The paper is organised as follows. In Section 2, we introduce the ion-kinetic hybrid-Vlasov code Vlasiator and how the Vlasov equation is solved, with additional modifications implemented for the analysis of electron distribution functions. Section 3 describes how our electron simulation is set up from fields and moments modelled by an ion-kinetic simulation. In Section 4 we perform rigorous validation and stability tests for our electron solver, and in Section 5 we present some electron distribution functions achieved by running our solver on a test dataset, comparing them with existing literature. Finally, Section 6 draws conclusions of our analysis and lays out a plan for future research approaches.

2 The Vlasiator ion-kinetic hybrid-Vlasov code

Vlasiator (von Alfthan et al., 2014; Palmroth et al., 2018) is, at the present time, the only hybrid-Vlasov code capable of simulating the global magnetospheric system of the Earth, accounting for ion-kinetic effects on spatial and temporal scales which model both magnetopause and magnetotail dynamics. Vlasiator solves the Vlasov equation for particle distribution functions discretized on cartesian grids, with closure provided by Ohm's law augmented by the Hall term. Each particle population is described using a uniform cartesian three-dimensional velocity space grid (3V) with a resolution chosen to accurately model the solar wind inflow Maxwellian distribution and with extents chosen to encompass heated ion populations associated with the magnetosheath and flux transfer events. A standard Vlasiator global run proton velocity-space grid has a resolution of $30\,\mathrm{km\,s^{-1}}$, extending between $\pm 4020\,\mathrm{km\,s^{-1}}$. To constrain computational cost and memory usage, those parts of

https://doi.org/10.5194/angeo-2020-31
Preprint. Discussion started: 2 June 2020


Annales Geophysicae Discussions Open Access EGU

the velocity distribution function which have a phase-space density below a sparsity threshold are discarded, except for buffer regions which allow the correct growth of the VDF in these parts (von Alfthan et al., 2014). The proton sparsity threshold is usually set to a value between 10^{-17} and $10^{-15}\,\mathrm{m}^{-6}\,\mathrm{s}^{3}$.

In the spatial domain, Vlasiator can be run in 1D, 2D, or 3D, with 2D the most usual choice in order to evaluate global dynamics. Simulations have used spatial resolutions of, e.g., $\Delta x = 228\,\mathrm{km}$ or $\Delta x = 300\,\mathrm{km}$, enough to accurately model ion cyclotron waves though not resolving the ion inertial length in all regions of the simulation domain. Large-scale global 3D runs will be made possible in the near future by adaptive mesh refinement (AMR), using non-uniform cell sizes in the spatial domain, thus cutting down on the computational cost of the simulation.

Vlasiator models standard collisionless space plasmas dominated by protons but can also model other particle species in the same self-consistent simulation. However, until now, the electron population has been treated in the usual way of implementing it as a massless charge-neutralizing fluid. This method does not track the evolution of electrons beyond assuming charge neutrality, and therefore, these standard Vlasiator simulations cannot be used to infer electron dynamics. This paper presents a novel approach for investigating how a global plasma current structure can influence electrons with limited self-consistency enforced through plasma oscillation and current densities. The method focuses on the evolution of accurately modelled velocity distribution functions based on global plasma dynamics and structures evolved by the hybrid model. The spatial scales used in Vlasiator are not sufficient to resolve in detail small-scale phenomena such as electron-dominated reconnection, but this balances out with a realistic representation of global structures and asymmetries of the whole magnetosphere.

2.1 Solving the Vlasov equation

Vlasiator uses the hybrid-Vlasov ion approach to model the near-Earth space plasma environment. The full six-dimensional (6D) phase space density $f_s(\mathbf{x}, \mathbf{v}, t)$, with $\mathbf{x}$ the ordinary space variable, $\mathbf{v}$ the velocity space variable, and t the time variable, for each ion species s of charge q_s and mass m_s is evolved in time using the Vlasov equation (1). The electric and magnetic fields, denoted $\mathbf{E}$ and $\mathbf{B}$ respectively, are evolved using Maxwell's equations: Faraday's Law (2), Gauss's Law (3) and Ampère's Law (4), in which μ_0 and ε_0 are the vacuum permeability and permittivity, respectively, and $\mathbf{j}$ is the total current density. The solenoid condition in Gauss's Law (3) is ensured via divergence-free magnetic field reconstruction (Balsara, 2009). In the hybrid approach, electrons are assumed to maintain plasma neutrality, resulting in the charge density ρ_q in Gauss's law vanishing. In the Darwin approximation, also used in many hybrid codes, propagation of light waves is neglected by removing the displacement current term $\varepsilon_0 \frac{\partial \mathbf{E}}{\partial t}$ in Ampère's law (4). The Vlasiator field solver follows the staggered-grid approach of Londrillo and Del Zanna (2004), and is described in detail in Palmroth et al. (2018).

https://doi.org/10.5194/angeo-2020-31
Preprint. Discussion started: 2 June 2020

Annales Geophysicae Discussions
Open Access
EGU

$$\frac{\partial f_s}{\partial t} + \mathbf{v} \cdot \frac{\partial f_s}{\partial \mathbf{x}} + \frac{q_s}{m_s} (\mathbf{E} + \mathbf{v} \times \mathbf{B}) \cdot \frac{\partial f_s}{\partial \mathbf{v}} = 0. \tag{1}$$

$$\nabla \times \mathbf{E} = -\frac{\partial \mathbf{B}}{\partial t} \tag{2}$$

$$\nabla \cdot \mathbf{B} = 0 \text{ and } \nabla \cdot \mathbf{E} = \frac{\rho_q}{\varepsilon_0} \tag{3}$$

$$\nabla \times \mathbf{B} = \mu_0 \left(\mathbf{J} + \varepsilon_0 \frac{\partial \mathbf{E}}{\partial t} \right) \tag{4}$$

The generalized Ohm's Law providing closure for the Vlasov system is

$$\mathbf{E} + \mathbf{V} \times \mathbf{B} = \frac{\mathbf{J}}{\sigma} + \frac{\mathbf{J} \times \mathbf{B}}{n_\mathrm{e} e} - \frac{\nabla \cdot \mathcal{P}_\mathrm{e}}{n_\mathrm{e} e} + \frac{m_\mathrm{e}}{n_\mathrm{e} e^2} \frac{\partial \mathbf{J}}{\partial t}, \tag{5}$$

where $\mathbf{V}$ is the plasma bulk velocity, σ is the conductivity, e is the elementary charge, n_e is the electron number density, and $\mathcal{P}_\mathrm{e}$ is the electron pressure tensor. In hybrid approaches of collisionless plasma, we can assume high conductivity, neglecting the first term on the right-hand side. In the limit of slow temporal variations, the electron inertia term (the last term on the right-hand side) also vanishes. The remaining two terms on the right-hand side of the equation are the Hall term, $\mathbf{J} \times \mathbf{B}/(n_\mathrm{e} e)$, and the electron pressure gradient term, $\nabla \cdot \mathcal{P}_\mathrm{e}/(n_\mathrm{e} e)$. In hybrid models, a true description of electron pressure is unavailable so it must be described via some approximation such as adiabatic, isothermal or polytropic electrons or a fixed ion-to-electron temperature ratio, or by neglecting the small electron pressure gradient term altogether. The standard ion-hybrid Vlasiator code supports isothermal fluid electrons but existing simulations have always set this temperature to zero. This along with assuming charge-neutrality (proton number density $n_\mathrm{p} = n_\mathrm{e}$) results in the ion-hybrid Vlasiator using the simplified MHD version of Ohm's Law with the Hall term included:

$$\mathbf{E} + \mathbf{V} \times \mathbf{B} = \frac{1}{e n_\mathrm{p} \mu_0} (\nabla \times \mathbf{B}) \times \mathbf{B}. \tag{6}$$

2.2 Implementing a global electron solver

In order to facilitate Vlasov simulation of electron distribution functions, the solvers used by Vlasiator must be extended. We will consider each term separately:

- Collisionless plasma physics assumes that electrons are fast enough to balance out any charge imbalance, and on the spatial scales involved in global simulations, we assume charge neutrality to hold as $\nabla \cdot \mathbf{E} = \frac{\rho_q}{\varepsilon_0} = 0$. This simplifies our electric field calculations significantly as we do not need to implement a Poisson electrostatic solver. This assumption is not expected to hold true on small spatial scales, but with grid resolutions $\gtrsim d_i$ it is considered a fair approximation.

- The last term in Ampère's law (4) is the displacement current, which is neglected in the Darwin approximation. However, electron motion can be very rapid and thus we now include this term in our model, though still maintaining static magnetic fields.

https://doi.org/10.5194/angeo-2020-31
Preprint. Discussion started: 2 June 2020

Annales Geophysicae Discussions
Open Access
EGU

- As our plasma remains collisionless, we maintain our assumption of infinite conductivity, and thus the $\mathbf{J}/\sigma$ term in the generalized Ohm's law (5) remains zero.
- The Hall term, $\mathbf{J} \times \mathbf{B}/(n_e e)$, is used to estimate the electron reference frame, and is discussed further below.
- The electron pressure gradient term models how spatial variation of electron pressure can lead to small imbalances of charge at e.g. shocks and reconnection sites. As it is a feature of only the hybrid approach, it is not included in our electron solver.
- The final term of the general Ohm's law is the electron inertia term. Much like with our choice of including the displacement current, we now include the electron inertia term in our solver.

As Vlasov methods do not propagate particles but rather evolve distribution functions, we now briefly explain the semi-Lagrangian method employed by Vlasiator (Palmroth et al., 2018). Vlasiator propagates distribution functions of particles following the SLICE-3D method (Zerroukat and Allen, 2012) and utilizing Strang splitting with advection (the second term of Vlasov's equation 1) and acceleration (the third term of Vlasov's equation 1) calculated one after the other with a Leapfrog offset of $\frac{1}{2}\Delta t$. For non-relativistic electrons, the advection step requires no adjustments, but the acceleration step must be adjusted to account for electron oscillation. For each time step, a Vlasov acceleration is evaluated with time step length Δt which is, amongst other things, limited to a maximal Larmor orbit gyromotion rotation of 22°. For each acceleration step, a transformation matrix is initialized as an identity matrix. This transformation matrix is updated with substepping of δ_{t_s} where each δ_{t_s} corresponds to a 0.1° Larmor gyration. Instead of applying linear acceleration by electric fields, a method similar to the Boris-push method (Boris, 1970) is applied, where first a transformation is performed to move to a frame in which electric fields vanish, then the rotation is applied, and then a frame transformation back to the original frame is added. In the standard hybrid formalism, the frame without electric fields is found via the MHD Ohm's law with the Hall term included (6). This Hall frame estimates the frame of reference of electrons, assuming electrons generate a current density which corresponds to the local magnetic field structure, in accordance with Ampère's law.

For electron dynamics to be modelled, electron gyration and plasma oscillation must both be considered. We limit the acceleration time step to a maximum of 22° of Larmor rotation or $22/360$ of a single plasma oscillation. The value of 22° is used to ensure our VDF remapping algorithm SLICE-3D remains stable and the value $22/360$ was chosen for equal resolution of both oscillations. The electron gyroperiod is $\tau_{ce} = 2\pi\omega_{ce}^{-1}$ and the plasma oscillation time is $\tau_{pe} = 2\pi\omega_{pe}^{-1}$, where the electron plasma frequency is

$$\omega_{pe} = \sqrt{\frac{n_e e^2}{\varepsilon_0 m_e}} \tag{7}$$

and the electron gyrofrequency is

$$\omega_{ce} = \frac{eB}{m_e}. \tag{8}$$

https://doi.org/10.5194/angeo-2020-31
Preprint. Discussion started: 2 June 2020


Annales Geophysicae Discussions Open Access EGU

In transformation matrix generation, substepping is constrained to a maximum of $\delta_{t_s} \leq \min(\tau_{pe}, \tau_{ce})/3600$. For each substep, a procedure similar to the hybrid method is applied, with the improvement that instead of performing gyration in the Hall frame (estimating the electron frame within the hybrid context) the gyration is performed in the actual substep-updated electron frame.

Electron oscillation is handled in parallel with gyration by tracking an additional cell-volume-averaged electric field component E_{J_e} which is itself derived from the small-scale electron oscillation. For each substep, we perform two parallel 4th order Runge-Kutta propagations. The first one is

$$\delta V_e = \delta_{t_s} \frac{e}{m_e} E_{J_e}, \tag{9}$$

tracking electron bulk velocity response δV_e to the E_{J_e} field. This simple acceleration term is in fact equal to evaluating current changes via the electron inertia term in Ohm's law with the E_{J_e} field included in the left-hand-side electric field. The second Runge-Kutta propagation tracks the evolution of the E_{J_e} field due to changing current density, according to the displacement current on the right-hand side of Ampère's law (4), whilst maintaining static magnetic fields. The $\nabla \times \mathbf{B}$ term in Ampère's law is fixed to the static input magetic fields. Thus, for each Runge-Kutta step, the electric field E_{J_e} is updated with

$$\delta E_{J_e} = \delta_{t_s} \left(\frac{\nabla \times \mathbf{B}}{\varepsilon_0 \mu_0} - \frac{\mathbf{J}}{\varepsilon_0} \right) \tag{10}$$

$$= \delta_{t_s} \left(\frac{\nabla \times \mathbf{B}}{\varepsilon_0 \mu_0} - \frac{eV_p n_p - eV_e n_e}{\varepsilon_0} \right) \tag{11}$$

$$= \delta_{t_s} c^2 \left(\nabla \times \mathbf{B} + \mu_0 e \left(n_e V_e - n_p V_p \right) \right) \tag{12}$$

where c is the speed of light, and $\mathbf{B}$, n_p and the proton bulk velocity V_p are assumed constant throughout the substep. Each of the four δV_e Runge-Kutta coefficients are updated with the latest estimate for δE_{J_e}, and vice versa. Values for E_{J_e} are stored between acceleration steps to ensure continuity of the oscillation. The change δV_e calculated via each Runge-Kutta step is then applied to the transformation matrix, allowing the solver to proceed to perform gyration in the electron frame of reference. The substepping procedure is visualized in Figure 1. Further details of the solver and advection methods in Vlasiator can be found in Palmroth et al. (2018).

After substepping is completed, the transformation matrix describing Vlasov acceleration is passed to the SLICE-3D algorithm, which decomposes the transformation into three cartesian shears and updates the velocity distribution function for the particle species.

3 Simulation setup

Modelling the evolution of electron distribution functions in response to global magnetic field structures requires input from the large-scale fields and moments of a Vlasiator simulation of near-Earth space. In this method introduction, we use a noon-midnight meridional-plane 2D-3V Vlasiator simulation as our test-case input data. This 2D-3V Vlasiator simulation has been used to investigate global and kinetic magnetospheric dynamics in multiple studies such as Palmroth et al. (2017); Hoilijoki et al. (2017); Juusola et al. (2018a, b); Hoilijoki et al. (2019b); Grandin et al. (2019); Akhavan-Tafti et al. (2020). It has solar

https://doi.org/10.5194/angeo-2020-31
Preprint. Discussion started: 2 June 2020

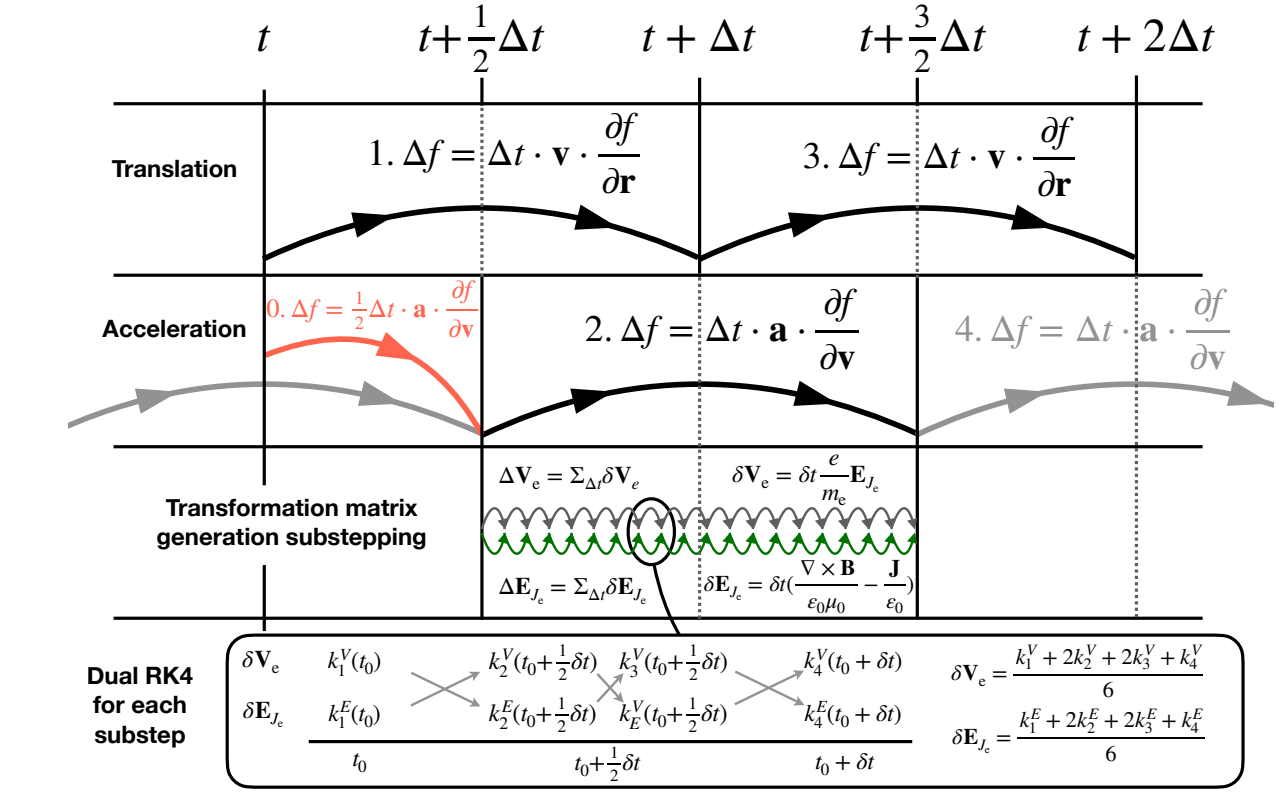

Figure 1. Electron solver procedure including substepping. At simulation start, a half-length acceleration step (0.) is performed. After that, translation (1,3,...) and acceleration (2,4,...) steps alternate in a Leapfrog approach. Each acceleration step applies a transformation matrix which is generated in substeps, each of which updates electron acceleration $\Delta\mathbf{V}_\mathrm{e}$ and electric field change $\Delta\mathbf{E}_{J_\mathrm{e}}$. Each of these updates is performed via a dual Runge-Kutta 4 algorithm over step lengths δt with Runge-Kutta coefficients $k^E_{1\ldots4}$ and $k^V_{1\ldots4}$

wind values of $\beta = 0.7$, magnetosonic Mach number $\mathrm{M_{ms}} = 5.6$, Alfvén Mach number $\mathrm{M_A} = 6.9$, proton number density $n_\mathrm{p} = 1\,\mathrm{cm}^{-3}$, and solar wind speed $\mathbf{u}_\mathrm{sw}$ along the $\hat{e}_x$ (Earth–Sun) direction with $u_{\mathrm{sw,x}} = -750\,\mathrm{km\,s}^{-1}$, simulating fast solar wind conditions and ensuring efficient simulation initialization. The simulation input interplanetary magnetic field is purely southward with $B_z = -5\,\mathrm{nT}$ and the Earth's magnetic dipole is a $\hat{e}_z$-aligned line dipole scaled to result in a realistic magnetopause standoff distance (Daldorff et al., 2014). The simulation has an inner boundary at $3 \cdot 10^6\,\mathrm{m} \approx 4.7$ Earth radii, modelled as a perfectly conducting sphere.

We do not model electrons throughout the whole global domain, choosing instead a region of interest to reduce the computational cost, though our method is designed to work with any subset of and up to the whole global domain. We choose a region from the magnetotail with $70 \times 1 \times 40$ simulation cells in the X, Y, and Z directions, respectively. The subregion extent is from $X_- = -75.6 \cdot 10^6\,\mathrm{m}$ to $X_+ = -54.6 \cdot 10^6\,\mathrm{m}$, from $Y_- = -0.15 \cdot 10^6\,\mathrm{m}$ to $Y_+ = +0.15 \cdot 10^6\,\mathrm{m}$, and from $Z_- = -6 \cdot 10^6\,\mathrm{m}$ to

https://doi.org/10.5194/angeo-2020-31
Preprint. Discussion started: 2 June 2020

Annales Geophysicae Discussions

$Z_+ = +6{\cdot}10^6\,\mathrm{m}$. Within this domain, visualized with a small rectangle in Figure 2a, the electron plasma period τ_{pe} ranges from $\sim 0.7\,\mathrm{ms}$ in the magnetotail plasma sheet up to $\sim 2.5\,\mathrm{ms}$ in the near-plasmasphere lobes. The electron gyroperiod τ_{ce} ranges from $\sim 14\,\mathrm{ms}$ in most of the lobes up to $\sim 770\,\mathrm{ms}$ at a tail current sheet X-line site. For the selected domain, we read in the Vlasiator ion-hybrid simulation proton moments, cell-face-average magnetic field components and cell-edge-average electric field components (the latter being used by the staggered-grid field solving algorithm from Londrillo and Del Zanna 2004). Both protons and electrons for the electron simulation are initialized from the read moments as Maxwellian distribution functions, with electron bulk velocity including the Hall term of generalized Ohm's law. The distributions are discretized onto Vlasiator velocity meshes, with the electron velocity mesh consisting of 400^3 cells, extending from $-4.2 \cdot 10^7$ to $+4.2 \cdot 10^7\,\mathrm{m\,s^{-1}}$ in each direction, resulting in an electron velocity space resolution of $210\,\mathrm{km\,s^{-1}}$. The electron VDF sparsity threshold was set to $10^{-21}\,\mathrm{m^{-6}\,s^3}$, ensuring good representation of the main structure of the VDF. Re-mapping input run Vlasiator proton VDFs as Maxwellians does not affect the simulation results as the electron solver only considers the proton number density and bulk velocity for current density calculations. For each simulation cell, we use the Balsara (2009) approach for calculating cell-average volumetric magnetic fields and respective derivatives. Our electron solver uses volumetric field derivatives for calculating $\nabla \times \mathbf{B}$. During our simulation run of up to $t_{\mathrm{max}} = 1.0\,\mathrm{s}$, the magnetic fields and proton moments are kept static.

Discretizing a hot and dense electron distribution onto a cartesian grid is numerically challenging without using vast amounts of memory. As portions of our simulation domain have proton temperature up to $10^8\,\mathrm{K}$, we use an empirical estimate of $T_{\mathrm{i}}/T_{\mathrm{e}} \sim 4$ as magnetosheath temperature ratios are usually around 4 to 12 (Wang et al., 2012). Paterson and Frank (1994), Hoshino et al. (2001), Artemyev et al. (2011), and Grigorenko et al. (2016) show similar proton-electron temperature ratios in the magnetotail. In order to constrain the extent of our velocity space and numerical requirements of our solver, we implement our electrons with a mass of 10 times the true electron mass, resulting in an ion-to-electron mass ratio of $m_{\mathrm{i}}/m_{\mathrm{e}} = 183.6$. As mentioned above, we calculate the required electron bulk velocity for each cell using the local volumetric (cell-average) derivatives so that the ion and electron fluxes in each cell correspond with the current density **J** required for fulfilling Ampère's law (4) (with the displacement current neglected at initialization). This is equal to performing a transformation to the Hall frame of reference. Proton densities, magnetic field lines, proton temperatures, proton bulk velocities and electron bulk velocities calculated for simulation initialization are shown in Figure 2 along with an overview of the input Vlasiator simulation and the selected electron sub-domain.

4 Solver performance

4.1 Single-cell stability of electron oscillation

To validate the performance of our electron solver, we performed single-cell tests, with resultant electron bulk velocities V_{e} and plasma oscillation electric fields $E_{J_{\mathrm{e}}}$ shown in Figure 3. These single-cell tests did not have magnetic field curvature or an ion population present, resulting in the electron motion oscillating around a stability point at $V_{\mathrm{e}} = 0$ and $E_{J_{\mathrm{e}}} = 0$. We set the electron number density to $n_{\mathrm{e}} = 0.1\,\mathrm{cm^{-3}}$ and the magnetic field to $B_x = 20\,\mathrm{nT}$ (panels a through d) or $B_x = 200\,\mathrm{nT}$ (panels e and f). We set an initial velocity perturbation of $V_{\mathrm{e},0} = (-100, -150, 200)\,\mathrm{km\,s^{-1}}$, close to but below our electron velocity

https://doi.org/10.5194/angeo-2020-31
Preprint. Discussion started: 2 June 2020

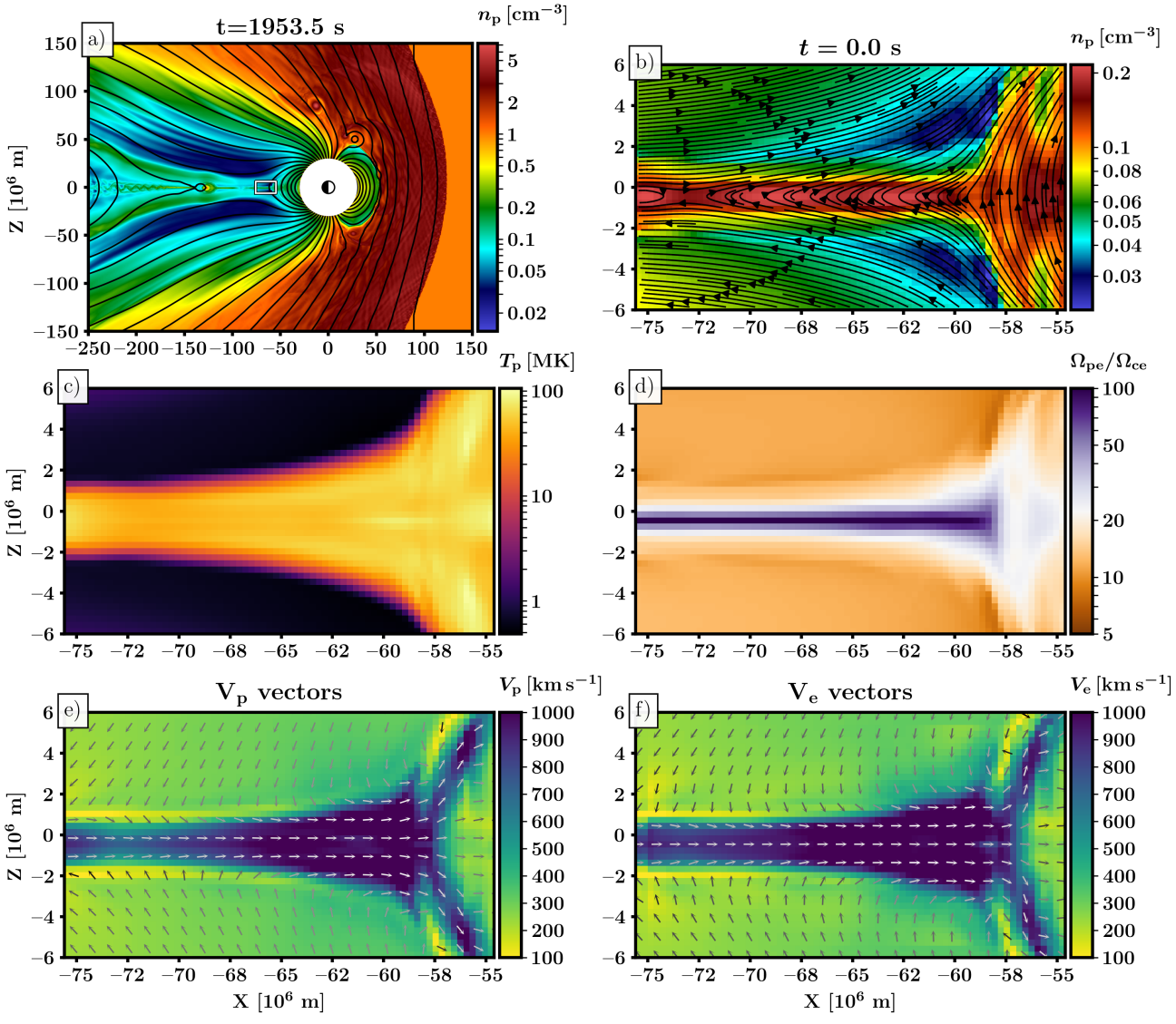

Figure 2. Simulation box initialization values. Panel a): Zoom-in to the central 16% section of the Vlasiator input simulation with plasma number density overlaid with magnetic field lines. A small rectangle in the magnetotail region indicates the electron simulation domain (panels b–f). Panel b): proton number density overlaid with magnetic field lines. X-line topology is visible at $X \sim -73 \cdot 10^6\,\mathrm{m}$ $Z \sim -0.5 \cdot 10^6\,\mathrm{m}$. Panel c): Proton temperature as a scalar. Electron initialization temperatures are scaled down by a constant factor 4. Panel d): ratio of electron plasma and gyrofrequencies. Panels e) and f): Proton and electron bulk velocity magnitudes with in-plane directions indicated with vectors.

resolution of $\Delta v = 210\,\mathrm{km\,s^{-1}}$. As can be seen from Figure 3, the electron oscillatory motion is well resolved and remains stable over an extended period. In panels e) and f) where the magnetic field strength was artificially increased in order to set

https://doi.org/10.5194/angeo-2020-31
Preprint. Discussion started: 2 June 2020

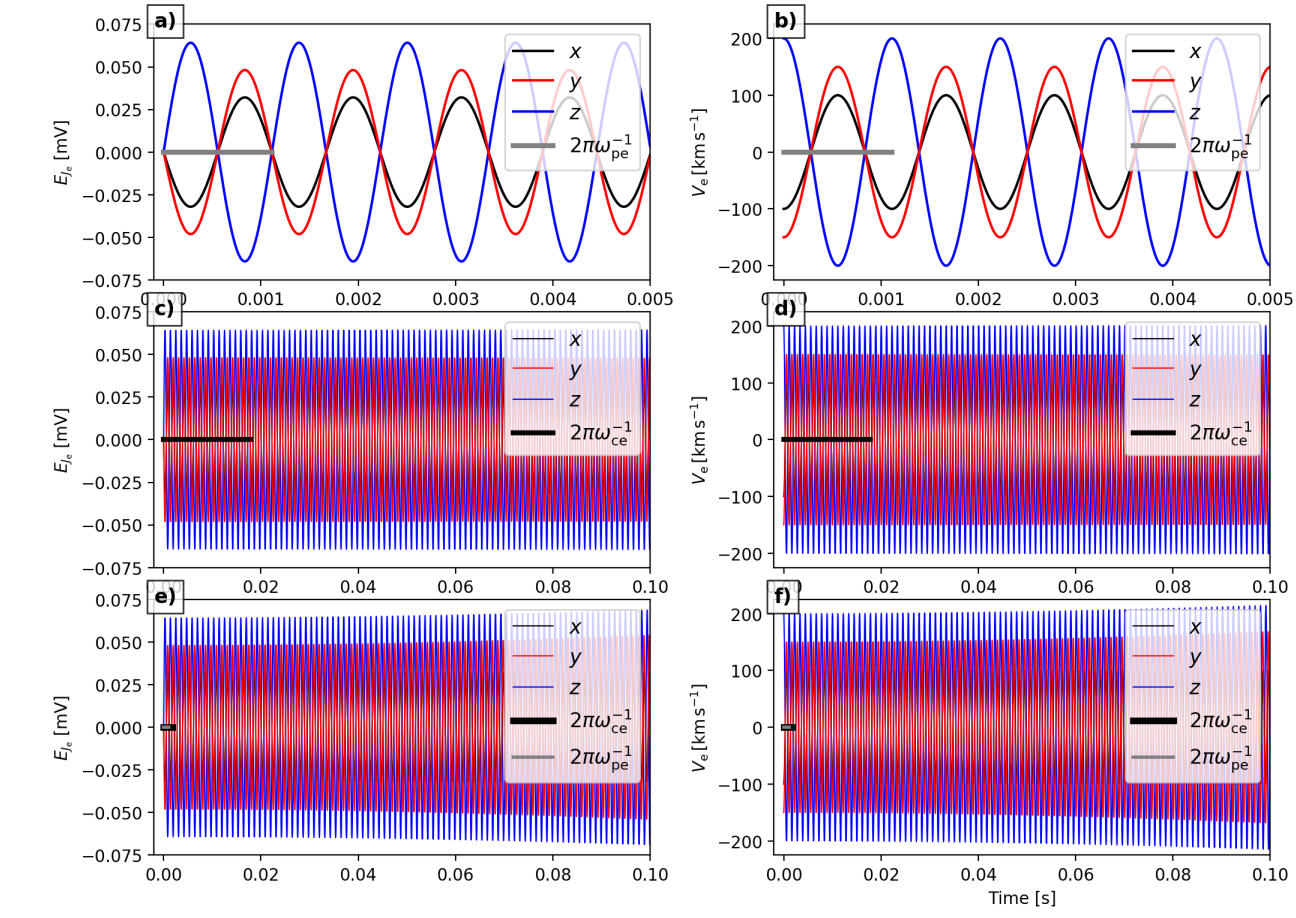

Figure 3. Graphs of solver stability in relation to electron plasma oscillation and gyromotion. Note the different time axes used. Panels a), c), and e): Oscillation electric field E_{J_e} components. Panels b), d), and f): Electron bulk velocity V_e components. Panels a) and b) graph values in relation to the electron plasma oscillation period (indicated with a thick grey bar) and panels c) and d) in relation to the electron gyroperiod (indicated with a thick black bar), with a background magnetic field of $B = 20\,\mathrm{nT}$. Panels e) and f) showcase a simulation with a magnetic field of $B = 200\,\mathrm{nT}$, resulting in the gyro- and oscillatory motions interacting over multiple periods.

4.2 Dispersion relation analysis

Although our method is geared towards solving electron motion at coarse spatial resolutions, to further validate the solver, a wave dispersion test was run (Kilian et al., 2017; Kempf et al., 2013). As waves are a collective, emergent phenomenon of

https://doi.org/10.5194/angeo-2020-31
Preprint. Discussion started: 2 June 2020

Annales Geophysicae Discussions
Open Access
EGU

the kinetic simulation approach, a correct reproduction of wave dispersion behaviour is a good indicator of correct physical behaviour of the simulation system.

Two 1D-simulation setups with a spatial grid resolution of $\Delta x = 300\,\mathrm{m}$ (= 0.01 d_e) and $N_x = 1000$ cells were initialized with an electron number density of $n_\mathrm{e} = 0.4 \cdot 10^6\,\mathrm{m}^{-3}$, an electron temperature of $T_\mathrm{e} = 2.5\,\mathrm{MK}$, and a magnetic field magnitude of 50 nT. In one simulation, the magnetic field direction was chosen to coincide with the extended simulation direction (resulting in parallel plasma wave modes to be resolved), in the other one, the magnetic field was set up perpendicular to the long dimension, resulting in perpendicular mode resolution. The plasma had zero bulk velocity in the simulation frame, with an added white noise velocity fluctuation of $\tilde{v} = 1000\,\mathrm{m/s}$. The simulation was run for 0.037 seconds (433 ω_pe^{-1}).

Figure 4 shows the dispersion data resulting from spatial and temporal Fourier transform (using a von Hann window). Overlaid are analytic dispersion curves for the Langmuir wave (black dashed curve) and electron Bernstein modes (black solid curves). The wave behaviour in the simulation shows good agreement in both parallel and perpendicular directions. One noteworthy additional feature visible in the parallel direction (Figure 4a) is the presence of an entropy wave feature at low wave number k and angular frequency ω that shows a quantization consistent with the electron velocity space resolution.

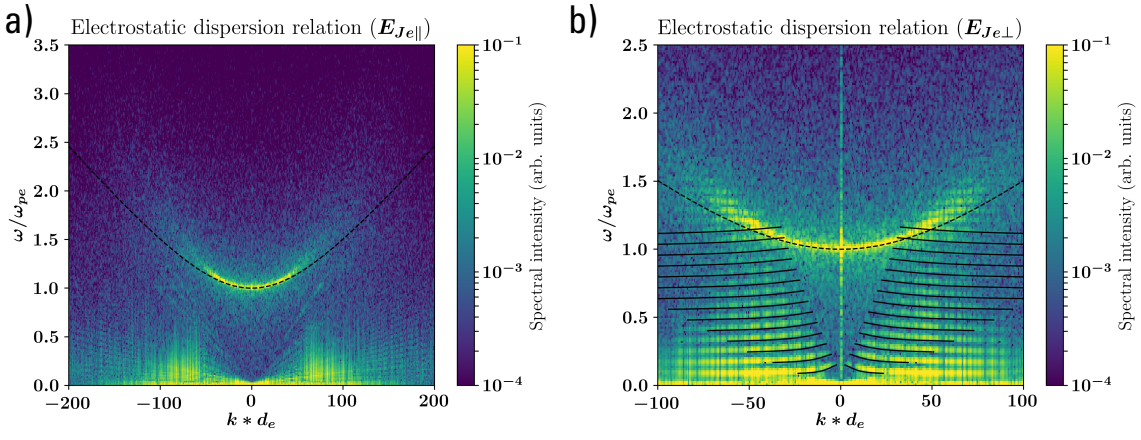

Figure 4. Dispersion analysis of the electron solver in a 1D test case with an axis-parallel (panel a) and axis-perpendicular (panel b) magnetic field. The colormap shows the spatiotemporal Fourier transform of $E_{J_\mathrm{e},\parallel}$ (panel a) and $E_{J_\mathrm{e},\perp}$ (panel b) overlaid with analytical solutions for the Langmuir wave (black dashed curve) and Bernstein modes (black solid curves).

4.3 Stability within larger simulation domain

We also evaluate the stability of our solver over the larger simulated domain described in Section 3, with initialization values derived from the Vlasiator hybrid-Vlasov simulation. These graphs are shown in Figure 5. Panels a) through e) show the evolution of electron temperature values over a simulation of 1.0 s, covering hundreds of electron plasma periods and, for the most part, tens of gyroperiods. We evaluate minimum, maximum, mean, and median values for total, $\mathbf{B}$-parallel, and $\mathbf{B}$-perpendicular electron temperatures. The system is seen to relax somewhat towards a final state, though some evolution is

https://doi.org/10.5194/angeo-2020-31
Preprint. Discussion started: 2 June 2020

Annales Geophysicae Discussions
Open Access
EGU

still apparent at the end of the simulation, possibly due to boundary effects. The maximum temperature plot in panel b) is of particular interest as the hottest plasma cells appear to diffuse into their surroundings until $t \sim 0.4$ s when dynamic gyration processes overtake this temperature diffusion with perpendicular heating. In panels f) through i) of Figure 5 we show how the instantaneous plasma oscillation electric fields E_{J_e} are well-behaved throughout the simulation box, converging towards stable values. We note that as E_{J_e} fields oscillate around zero, the averages are indeed zero throughout (not shown) and the values used for inferring minimum, maximum, mean and median values are instantaneous values from a arbitrary phase of the oscillation. Finally in panel j) we show the normalized current density $\mathbf{J}$ departure from the balance current $\mathbf{J_B} = \frac{\nabla \times \mathbf{B}}{\mu_0}$ which would be required to maintain the magnetic field structure according to Ampère's law (4). This metric is seen to also stabilize, mostly at values well below unity. We expect the maximum value outliers to be due to locally small values of $\mathbf{J_B}$.

As part of our evaluation of solver stability, we performed a comparison run where our electron solver performed the rotation transformation corresponding with gyromotion in the Hall frame instead of in the substep-associated electron bulk frame. This transformation choice resulted in unstable growth of, in particular, E_{J_e}, as could be expected (not shown).

5 Results

A selection of results from the electron simulation after 1.0 s of evolution is presented in Figure 6. Panel a) shows the evolved electron temperature anisotropy $T_{\perp,\mathrm{e}} T_{\parallel,\mathrm{e}}^{-1}$, and panel b) displays the maximum of instantaneous values of E_{J_e}, taken over 10 measurements at 0.05 s intervals near the end of the simulation. Panels c) through n) of Figure 6 show parallel and perpendicular projections of electron VDFs at virtual spacecraft (VSC) [1] through [6], with positions of VSC indicated in panels a) and b).

Figure 6a shows how temperature anisotropy $T_{\perp,\mathrm{e}} T_{\parallel,\mathrm{e}}^{-1}$ indicates parallel energization in the low-density regions adjacent to the plasma sheet boundary layer (PSBL) and perpendicular energization adjacent to the X-line and within the tailmost region of the magnetosphere. As we have bulk flows of both ions and electrons towards the tail current sheet, some of this heating can be attributed to betatron acceleration as electrons convect towards stronger magnetic fields just adjacent to the actual high-beta plasma sheet.

The maximum of instantaneous values of E_{J_e}, shown in Figure 6b, indicate that the strongest electron oscillations on our simulated scales are found in or near the PSBL, which would be consistent with observations of electron-driven waves in the PSBLOnsager et al. (1993). Some increase in E_{J_e} is seen also at the X-line location, but not in other parts of the current sheet. We note that the X-line included in this simulation was not actively reconnecting.

The temperature anisotropies found in the near-Earth tail region of our simulation are mostly in the 0.5…1.5 range. Artemyev et al. (2014) reported on Cluster observations of electron temperature anisotropies ranging from 0.8…1.6 and centered around ~ 1.1, in agreement with our results, though their observations were gathered between $-20\,R_\mathrm{E} < X < -15\,R_\mathrm{E}$ ($-127 \cdot 10^6 < X < 96 \cdot 10^6$ m).

Parallel heating near the magnetotail plasma sheet has been reported to coincide with bi-directional electron distributions (Hada et al., 1981) with temperature ratios going up to 2–3, as in our simulation. Our VSC [2] and [5] show clear bi-directional distributions. Due to our static background magnetic field, our parallel heating cannot be due to conventional Fermi accelera-

https://doi.org/10.5194/angeo-2020-31
Preprint. Discussion started: 2 June 2020

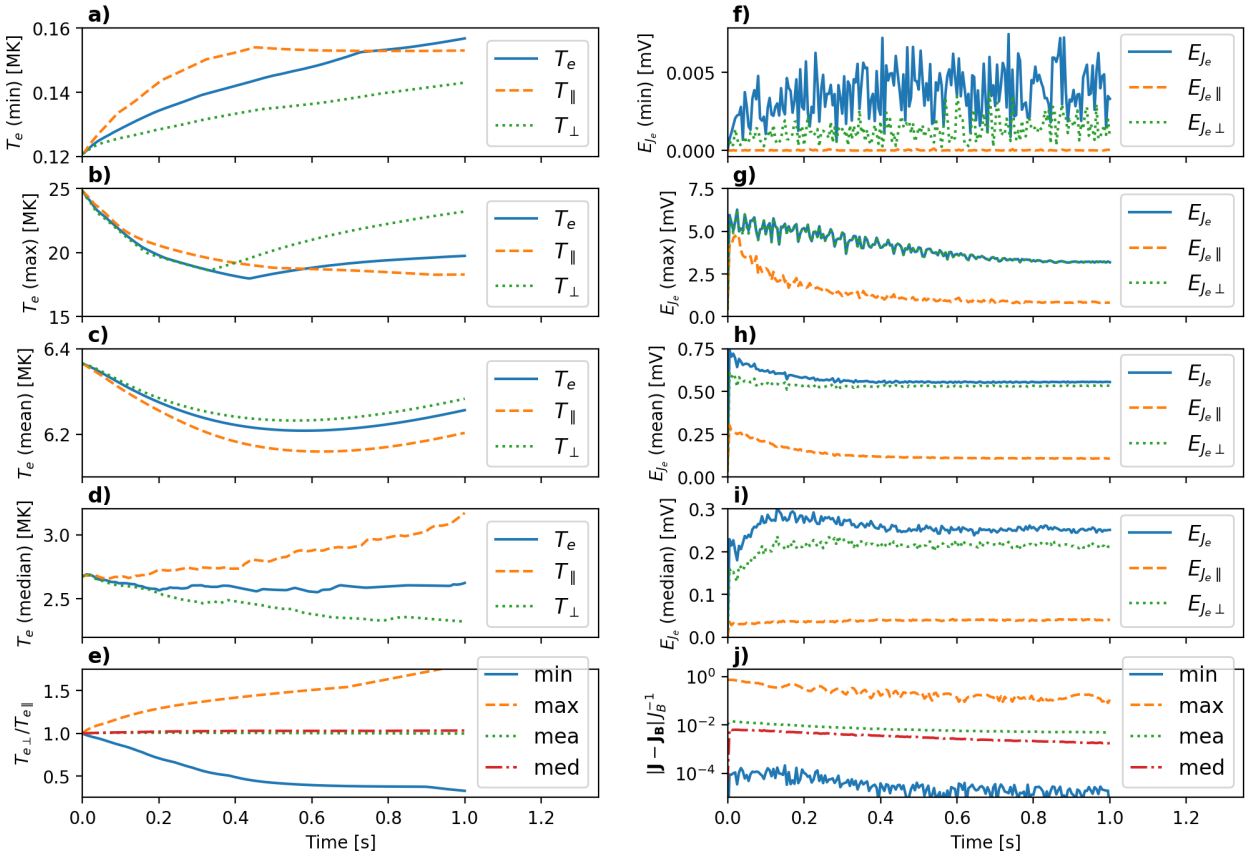

Figure 5. Evolution of electron and solver parameters over the whole simulation domain. Panels a) through d): Minimum, maximum, mean, and median values for electron temperature T_e and its components parallel and perpendicular to the local magnetic field. Panel e): Minimum, maximum, mean, and median values for electron temperature anisotropy. Panels f) through i): Minimum, maximum, mean, and median values for the plasma oscillation electric field E_{J_e} and its components parallel and perpendicular to the local magnetic field. Panel j): Minimum, maximum, mean, and median normalized values for current density $\mathbf{J}$ deviation from the value $\mathbf{J_B} = \frac{\nabla\times\mathbf{B}}{\mu_0}$ required by the local magnetic field.

tion. However, Hada et al. (1981) propose that adiabatic plasma processes where curvature drifts dominate over gradient drifts (Yamamoto and Tamao, 1978) can lead to significant parallel heating. Our VSC [1] is from close to the X-line and shows
310 parallel elongation of the central part of the distribution, reminiscent of the football or shifted-football distributions of Figure 2 of Hoshino et al. (2001).

Asano et al. (2006) describe streaming 500 eV electrons at the PSBL, associated with a substorm event and variation of B_y, especially at small scales. Scaling with our electron mass, this corresponds to approximately $4000\,\mathrm{km\,s^{-1}}$ electron velocities, which is reasonably within the range of our VDFs in Figure 6. We note that our simulation produces a background B_y profile

https://doi.org/10.5194/angeo-2020-31
Preprint. Discussion started: 2 June 2020

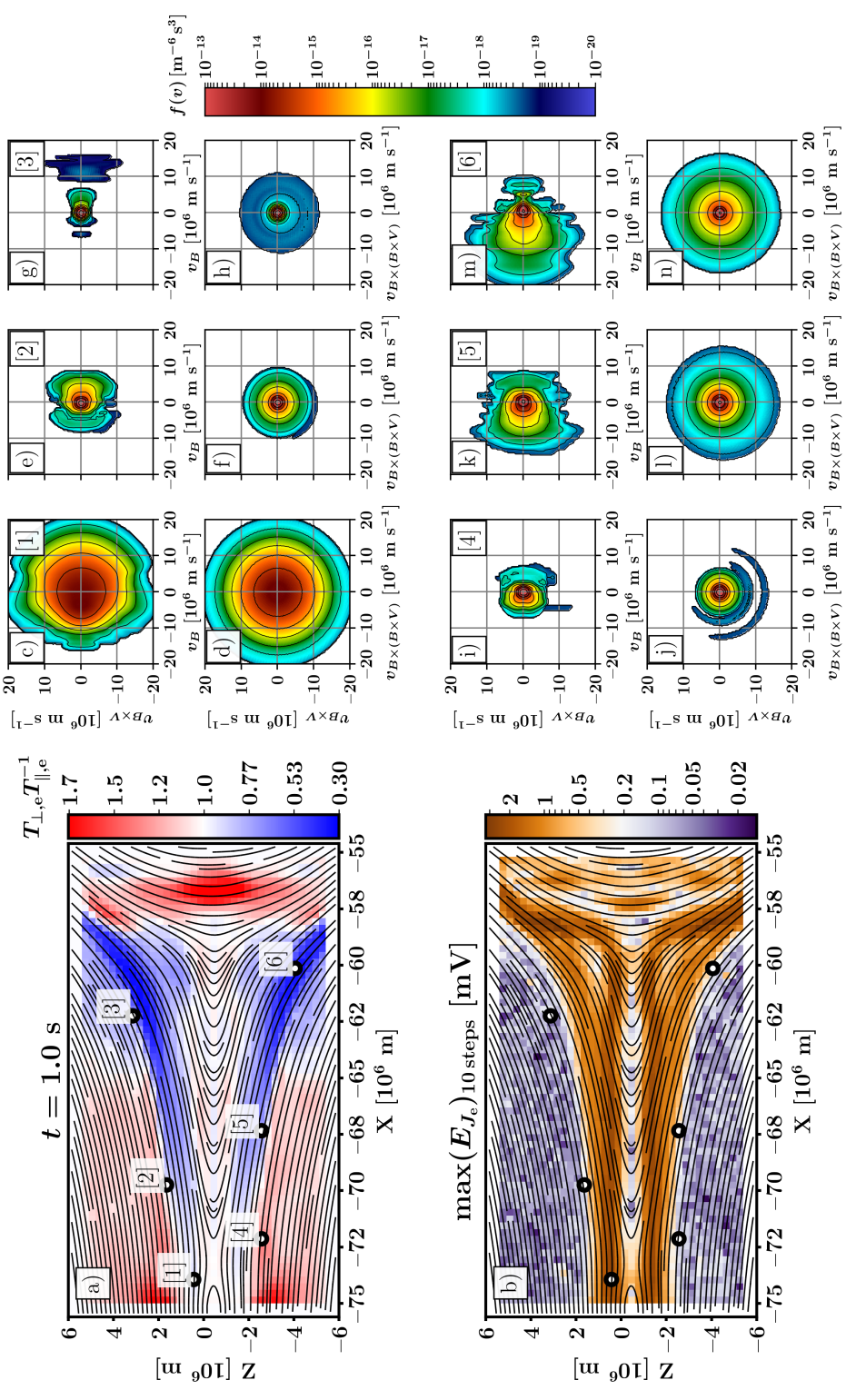

Figure 6. Electron properties and velocity distribution functions after 1.0 s of simulation. Panel a) Electron temperature anisotropy $T_{\perp,e}T_{\parallel,e}^{-1}$ overlaid with magnetic field lines and six virtual spacecraft locations, labelled [1]–[6]. Panel b): Maximum value for displacement current E_{J_e}, taken over 10 measurements at 0.05 s intervals near the end of the simulation. Panels c) through n): electron velocity distribution function projections into the parallel v_B and $v_{V\times B}$ or perpendicular $v_{B\times(B\times V)}$ and $v_{V\times B}$ planes. Each virtual spacecraft is indicated by the number in the parallel VDF panel with the panel below showing the corresponding perpendicular VDF for the same virtual spacecraft.

https://doi.org/10.5194/angeo-2020-31
Preprint. Discussion started: 2 June 2020


Annales Geophysicae Discussions

with ∇B_y in agreement with Figure 4 of Asano et al. (2006) (not shown), on top of which the streaming electrons are observed. Onsager et al. (1991) describe a simple 2-D Liouville model for the PSBL, as well as some ISEE-1 and ISEE-2 observations supporting their model. The formation mechanisms of eVDFs in Onsager et al. (1991) are listed as time-of-flight, energy conservation and magnetic moment conservation, which are included in our model, though we perform a more robust evaluation of plasma oscillation interplay with gyration. The eVDFs shown in their Figure 4 agree with e.g. our VSC [1], [2], [5], and [6]. We also note our VSC [3] displaying a disjoint parallel beam, matching the ISEE-2 observations in Figure 5 of Onsager et al. (1991).

Observations of perpendicular crescents are shown in MMS data in Burch et al. (e.g. 2016b, 2019) at electron diffusion regions (EDRs), in conjunction with dayside magnetopause reconnection sites. These observed structures are produced at very small spatial scales, not captured by our current model. We do, however, observe similar agyrotropic crescents in our results further out (in particular in Figure 6j), suggesting successful capture of a level of electron dynamics. Something akin to a parallel electron crescent (Burch et al., 2016b) can be seen in Figure 6c, and bi-directional distributions as reported in Figures 6 and 7 of Burch and Phan (2016) are qualitatively similar to our Figures 6k and m.

6 Conclusions

In this method paper we have presented a novel approach to investigating electron distribution function dynamics in the context of global ion-hybrid field structures. Our method exploits global dynamics provided by hybrid-Vlasov simulations in order to evaluate the response of gyrating and plasma oscillating electrons to global magnetic field structures.

We have shown our solver to behave in a stable manner, resolving electron inertia and updating a responsive electric field E_{J_e} derived from the displacement current. If run at much finer spatial resolutions, our model replicates Langmuir waves and electron Bernstein modes. Electron temperatures evolve in response to the field structure but do not experience uncontrolled growth. Our sample simulation produces multiple features associated with spacecraft observations of VDFs, such as parallel acceleration, bi-directional distributions, and perpendicular crescents.

Our model has several built-in limitations as it does not treat electrons as a fully self-consistent species. Magnetic fields gathered from the Vlasiator simulation are kept constant and thus force electron bulk motion to adhere to the required current density structure. As the initialization information is gathered from a hybrid-Vlasov simulation, it has a spatial resolution far below that required for resolving electron-scale waves such as whistlers, Bernstein waves and chorus waves. Scattering of electrons via these missing waves is somewhat accounted for by initializing every simulation from a Maxwellian isotropic distribution. These features together limit the applicability of the model to short periods of time. On the other hand, our model is efficient, taking only 80 thousand CPU hours to perform the sample simulation presented in this paper. Thus, much larger spatial domains of investigation are easily achievable. The method builds on the efficiently parallelized Vlasiator codebase and will benefit from future numerical and computational improvements to Vlasiator solvers.

Our model can be applied to investigate electron dynamics on global spatial scales, with the current version applicable to 2D investigations, e.g., in the noon-midnight meridional plane. Electron velocity distribution functions generated by the model

https://doi.org/10.5194/angeo-2020-31
Preprint. Discussion started: 2 June 2020


Annales Geophysicae Discussions

can be used to investigate, e.g., energetic electron precipitation into the Earth's auroral regions. The model can be run for several different initialization time steps to evaluate long-term evolution of precipitating electron distributions. Li et al. (2020) observe electron Bernstein modes driven by perpendicular crescent distributions. As we have shown in Figures 4 and 6, with sufficient resolution we can reproduce electron Bernstein waves and agyrotropic electron distributions. Thus, we are in position to investigate this connection further in Vlasiator.

Future improvements to our model will allow simulation initialization from non-uniform 3D-3V Vlasiator meshes, allowing investigation of spatially three-dimensional topologies including tail plasma sheet clock angle tilt. A possible path of future investigation would be to upsample the initialization fields and moments in order to achieve better resolution, but we emphasize that the model does not attempt to solve electrons in a fully self-consistent manner as magnetic fields are still kept constant. Upscaling the input moments might not significantly improve plasma sheet density and temperature profiles. Increasing spatial resolution introduces numerous caveats including increased computational cost and possible charge imbalance resulting from spatially resolved electron oscillations, though our dispersion tests did not indicate such problems. If such imbalances arise from a future model, some method of solving Gauss' Law such as a Poisson solver should be implemented. A more detailed investigation into comparing electron VDFs and dynamics with observations is expected in a future study.

Code and data availability. Vlasiator (http://www.physics.helsinki.fi/vlasiator/, Palmroth, 2020) is distributed under the GPL-2 open source license at https://github.com/fmihpc/vlasiator/ (Palmroth and the Vlasiator team, 2020). Vlasiator uses a data structure developed in-house (https://github.com/fmihpc/vlsv/, Sandroos, 2019). The Analysator software (https://github.com/fmihpc/analysator/, Hannuksela and the Vlasiator team, 2020) was used to produce the presented figures. The run described here takes several gigabytes of disk space and is kept in storage maintained within the CSC – IT Center for Science. Data presented in this paper can be accessed by following the data policy on the Vlasiator web site.

Author contributions. MB wrote the manuscript and code description. MA assisted with data analysis and comparisons with observations. MB and TB devised the solver method and developed the model. UG performed the dispersion tests. MP is the PI of Vlasiator and leads the investigation. Other co-authors, especially YPK and MG, helped with finalization of the manuscript.

Competing interests. The authors declare that they have no conflict of interest.

Acknowledgements. We acknowledge The European Research Council for Starting grant 200141-QuESpace, with which the Vlasiator model (http://www.physics.helsinki.fi/vlasiator) was developed, and Consolidator grant 682068-PRESTISSIMO awarded for further development of Vlasiator and its use in scientific investigations. We gratefully acknowledge Academy of Finland grants number 309937-TEMPO and 312351-FORESAIL. PRACE (http://www.prace-ri.eu) is acknowledged for granting us Tier-0 computing time in HLRS Stuttgart, where

https://doi.org/10.5194/angeo-2020-31
Preprint. Discussion started: 2 June 2020

Annales Geophysicae Discussions
Open Access
EGU

Vlasiator was run in the HazelHen machine with project number 2014112573 and in the Hawk machine with project number 2019204998. The work of L.T. is supported by the Academy of Finland (grant number 322544).

https://doi.org/10.5194/angeo-2020-31
Preprint. Discussion started: 2 June 2020

Annales Geophysicae Discussions
Open Access
EGU

References

Akhavan-Tafti, M., Palmroth, M., Slavin, J. A., Battarbee, M., Ganse, U., Grandin, M., Le, G., Gershman, D. J., Eastwood, J. P., and Stawarz, J. E.: Comparative Analysis of the Vlasiator Simulations and MMS Observations of Multiple X-Line Reconnection and Flux Transfer Events, Accepted for publication in Journal of Geophysical Research (Space Physics), 125, 2020.

Artemyev, A. V., Baumjohann, W., Petrukovich, A. A., Nakamura, R., Dandouras, I., and Fazakerley, A.: Proton/electron temperature ratio in the magnetotail, Annales Geophysicae, 29, 2253–2257, https://doi.org/10.5194/angeo-29-2253-2011, 2011.

Artemyev, A. V., Walsh, A. P., Petrukovich, A. A., Baumjohann, W., Nakamura, R., and Fazakerley, A. N.: Electron pitch angle/energy distribution in the magnetotail, Journal of Geophysical Research: Space Physics, 119, 7214–7227, https://doi.org/10.1002/2014JA020350, 2014.

Asano, Y., Nakamura, R., Runov, A., Baumjohann, W., McIlwain, C., Paschmann, G., Quinn, J., Alexeev, I., Dewhurst, J. P., Owen, C. J., Fazakerley, A. N., Balogh, A., Rème, H., and Klecker, B.: Detailed analysis of low-energy electron streaming in the near-Earth neutral line region during a substorm, Advances in Space Research, 37, 1382–1387, https://doi.org/10.1016/j.asr.2005.05.059, 2006.

Balsara, D. S.: Divergence-free reconstruction of magnetic fields and WENO schemes for magnetohydrodynamics, Journal of Computational Physics, 228, 5040–5056, https://doi.org/10.1016/j.jcp.2009.03.038, 2009.

Bessho, N., Chen, L.-J. J., Shuster, J. R., and Wang, S.: Electron distribution functions in the electron diffusion region of magnetic reconnection: Physics behind the fine structures, Geophysical Research Letters, 41, 8688–8695, https://doi.org/10.1002/2014GL062034, 2014.

Bessho, N., Chen, L.-J. J., and Hesse, M.: Electron distribution functions in the diffusion region of asymmetric magnetic reconnection, Geophysical Research Letters, 43, 1828–1836, https://doi.org/10.1002/2016GL067886, 2016.

Birdsall, C. K. and Langdon, A. B.: Plasma physics via computer simulation, Taylor and Francis, New York, 2005.

Boris, J. P.: Relativistic plasma simulation-optimization of a hybrid code, in: Proc. Fourth Conf. Num. Sim. Plasmas, pp. 3–67, 1970.

Burch, J. L. and Phan, T. D.: Magnetic reconnection at the dayside magnetopause: Advances with MMS, Geophysical Research Letters, 43, 8327–8338, https://doi.org/10.1002/2016GL069787, 2016.

Burch, J. L., Moore, T. E., Torbert, R. B., and Giles, B. L.: Magnetospheric Multiscale Overview and Science Objectives, Space Science Reviews, 199, 5–21, https://doi.org/10.1007/s11214-015-0164-9, 2016a.

Burch, J. L., Torbert, R. B., Phan, T. D., Chen, L.-J., Moore, T. E., Ergun, R. E., Eastwood, J. P., Gershman, D. J., Cassak, P. A., Argall, M. R., Wang, S., Hesse, M., Pollock, C. J., Giles, B. L., Nakamura, R., Mauk, B. H., Fuselier, S. A., Russell, C. T., Strangeway, R. J., Drake, J. F., Shay, M. A., Khotyaintsev, Y. V., Lindqvist, P.-A., Marklund, G., Wilder, F. D., Young, D. T., Torkar, K., Goldstein, J., Dorelli, J. C., Avanov, L. A., Oka, M., Baker, D. N., Jaynes, A. N., Goodrich, K. A., Cohen, I. J., Turner, D. L., Fennell, J. F., Blake, J. B., Clemmons, J., Goldman, M., Newman, D., Petrinec, S. M., Trattner, K. J., Lavraud, B., Reiff, P. H., Baumjohann, W., Magnes, W., Steller, M., Lewis, W., Saito, Y., Coffey, V., and Chandler, M.: Electron-scale measurements of magnetic reconnection in space, Science, 352, https://doi.org/10.1126/science.aaf2939, 2016b.

Burch, J. L., Dokgo, K., Hwang, K. J., Torbert, R. B., Graham, D. B., Webster, J. M., Ergun, R. E., Giles, B. L., Allen, R. C., Chen, L. J., Wang, S., Genestreti, K. J., Russell, C. T., Strangeway, R. J., and Le Contel, O.: High-Frequency Wave Generation in Magnetotail Reconnection: Linear Dispersion Analysis, Geophysical Research Letters, 46, 4089–4097, https://doi.org/10.1029/2019GL082471, 2019.

Cattell, C., Dombeck, J., Wygant, J., Drake, J. F., Swisdak, M., Goldstein, M. L., Keith, W., Fazakerley, A., André, M., Lucek, E., and Balogh, A.: Cluster observations of electron holes in association with magnetotail reconnection and comparison to simulations, Journal of Geophysical Research (Space Physics), 110, A01211, https://doi.org/10.1029/2004JA010519, 2005.

https://doi.org/10.5194/angeo-2020-31
Preprint. Discussion started: 2 June 2020

Daldorff, L. K. S., Tóth, G., Gombosi, T. I., Lapenta, G., Amaya, J., Markidis, S., and Brackbill, J. U.: Two-way coupling of a global Hall magnetohydrodynamics model with a local implicit particle-in-cell model, Journal of Computational Physics, 268, 236–254, https://doi.org/10.1016/j.jcp.2014.03.009, 2014.

Daldorff, L. K. S., Tóth, G., Gombosi, T. I., Lapenta, G., Amaya, J., Markidis, S., and Brackbill, J. U.: Two-way coupling of a global Hall magnetohydrodynamics model with a local implicit particle-in-cell model, Journal of Computational Physics, 268, 236–254, https://doi.org/10.1016/j.jcp.2014.03.009, 2014.

Daughton, W., Roytershteyn, V., Karimabadi, H., Yin, L., Albright, B. J., Bergen, B., and Bowers, K. J.: Role of electron physics in the development of turbulent magnetic reconnection in collisionless plasmas, Nature Physics, 7, 539–542, https://doi.org/10.1038/nphys1965, 2011.

Deca, J., Divin, A., Lembège, B., Horányi, M., Markidis, S., and Lapenta, G.: General mechanism and dynamics of the solar wind interaction with lunar magnetic anomalies from 3-D particle-in-cell simulations, Journal of Geophysical Research: Space Physics, 120, 6443–6463, https://doi.org/10.1002/2015JA021070, 2015.

Deca, J., Divin, A., Henri, P., Eriksson, A., Markidis, S., Olshevsky, V., and Horányi, M.: Electron and Ion Dynamics of the Solar Wind Interaction with a Weakly Outgassing Comet, Physical Review Letters, 118, 205 101, https://doi.org/10.1103/PhysRevLett.118.205101, 2017.

Deca, J., Henri, P., Divin, A., Eriksson, A., Galand, M., Beth, A., Ostaszewski, K., and Horányi, M.: Building a Weakly Outgassing Comet from a Generalized Ohm's Law, Physical Review Letters, 123, 055 101, https://doi.org/10.1103/PhysRevLett.123.055101, 2019.

Dungey, J. W.: Interplanetary magnetic field and the auroral zones, Physical Review Letters, 6, 47–48, https://doi.org/10.1103/PhysRevLett.6.47, 1961.

Ergun, R. E., Holmes, J. C., Goodrich, K. A., Wilder, F. D., Stawarz, J. E., Eriksson, S., Newman, D. L., Schwartz, S. J., Goldman, M. V., Sturner, A. P., Malaspina, D. M., Usanova, M. E., Torbert, R. B., Argall, M., Lindqvist, P. A., Khotyaintsev, Y., Burch, J. L., Strangeway, R. J., Russell, C. T., Pollock, C. J., Giles, B. L., Dorelli, J. J. C., Avanov, L., Hesse, M., Chen, L. J., Lavraud, B., Le Contel, O., Retino, A., Phan, T. D., Eastwood, J. P., Oieroset, M., Drake, J., Shay, M. A., Cassak, P. A., Nakamura, R., Zhou, M., Ashour-Abdalla, M., and André, M.: Magnetospheric Multiscale observations of large-amplitude, parallel, electrostatic waves associated with magnetic reconnection at the magnetopause, Geophysical Research Letters, 43, 5626–5634, https://doi.org/10.1002/2016GL068992, 2016.

Escoubet, C. P., Fehringer, M., and Goldstein, M.: IntroductionThe Cluster mission, Annales Geophysicae, 19, 1197–1200, https://doi.org/10.5194/angeo-19-1197-2001, 2001.

Fargette, N., Lavraud, B., Øieroset, M., Phan, T. D., Toledo-Redondo, S., Kieokaew, R., Jacquey, C., Fuselier, S. A., Trattner, K. J., Petrinec, S., Hasegawa, H., Garnier, P., Génot, V., Lenouvel, Q., Fadanelli, S., Penou, E., Sauvaud, J. A., Avanov, D. L. A., Burch, J., Chand ler, M. O., Coffey, V. N., Dorelli, J., Eastwood, J. P., Farrugia, C. J., Gershman, D. J., Giles, B. L., Grigorenko, E., Moore, T. E., Paterson, W. R., Pollock, C., Saito, Y., Schiff, C., and Smith, S. E.: On the Ubiquity of Magnetic Reconnection Inside Flux Transfer Event-Like Structures at the Earth's Magnetopause, Geophysical Research Letters, 47, e86726, https://doi.org/10.1029/2019GL086726, 2020.

Grandin, M., Battarbee, M., Osmane, A., Ganse, U., Pfau-Kempf, Y., Turc, L., Brito, T., Koskela, T., Dubart, M., and Palmroth, M.: Hybrid-Vlasov modelling of nightside auroral proton precipitation during southward interplanetary magnetic field conditions, Annales Geophysicae, 37, 791–806, https://doi.org/10.5194/angeo-37-791-2019, 2019.

Grigorenko, E. E., Kronberg, E. A., Daly, P. W., Ganushkina, N. Y., Lavraud, B., Sauvaud, J.-A., and Zelenyi, L. M.: Origin of low proton-to-electron temperature ratio in the Earth's plasma sheet, Journal of Geophysical Research: Space Physics, 121, 9985–10,004, https://doi.org/10.1002/2016JA022874, 2016.

https://doi.org/10.5194/angeo-2020-31
Preprint. Discussion started: 2 June 2020

Hada, T., Nishida, A., Teresawa, T., and Hones Jr., E. W.: Bi-directional electron pitch angle anisotropy in the plasma sheet, Journal of Geophysical Research: Space Physics, 86, 11 211–11 224, https://doi.org/10.1029/JA086iA13p11211, 1981.

Hannuksela, O. and the Vlasiator team: Analysator: python analysis toolkit, Github repository, https://github.com/fmihpc/analysator/, 2020.

Harris, E. G.: On a plasma sheath separating regions of oppositely directed magnetic field, Il Nuovo Cimento, 23, 115–121, https://doi.org/10.1007/BF02733547, 1962.

Hesse, M., Kuznetsova, M., Schindler, K., and Birn, J.: Three-dimensional modeling of electron quasiviscous dissipation in guide-field magnetic reconnection, Physics of Plasmas, 12, 100 704, https://doi.org/10.1063/1.2114350, 2005.

Hesse, M., Liu, Y. H., Chen, L. J., Bessho, N., Kuznetsova, M., Birn, J., and Burch, J. L.: On the electron diffusion region in asymmetric reconnection with a guide magnetic field, Geophysical Research Letters, 43, 2359–2364, https://doi.org/10.1002/2016GL068373, 2016.

Hoilijoki, S., Ganse, U., Pfau-Kempf, Y., Cassak, P. A., Walsh, B. M., Hietala, H., von Alfthan, S., and Palmroth, M.: Reconnection rates and X line motion at the magnetopause: Global 2D-3V hybrid-Vlasov simulation results, Journal of Geophysical Research (Space Physics), 122, 2877–2888, https://doi.org/10.1002/2016JA023709, 2017.

Hoilijoki, S., Ergun, R. E., Schwartz, S. J., Eriksson, S., Wilder, F. D., Webster, J. M., Ahmadi, N., Le Contel, O., Burch, J. L., Torbert, R. B., Strangeway, R. J., and Giles, B. L.: Electron-Scale Magnetic Structure Observed Adjacent to an Electron Diffusion Region at the Dayside Magnetopause, Journal of Geophysical Research (Space Physics), 124, 10,153–10,169, https://doi.org/10.1029/2019JA027192, 2019a.

Hoilijoki, S., Ganse, U., Sibeck, D. G., Cassak, P. A., Turc, L., Battarbee, M., Fear, R. C., Blanco-Cano, X., Dimmock, A. P., Kilpua, E. K. J., Jarvinen, R., Juusola, L., Pfau-Kempf, Y., and Palmroth, M.: Properties of Magnetic Reconnection and FTEs on the Dayside Magnetopause With and Without Positive IMF B_x Component During Southward IMF, Journal of Geophysical Research (Space Physics), 124, 4037–4048, https://doi.org/10.1029/2019JA026821, 2019b.

Hoshino, M., Hiraide, K., and Mukai, T.: Strong electron heating and non-Maxwellian behavior in magnetic reconnection, Earth, Planets and Space, 53, 627–634, https://doi.org/10.1186/BF03353282, 2001.

Huang, S. Y., Jiang, K., Yuan, Z. G., Sahraoui, F., He, L. H., Zhou, M., Fu, H. S., Deng, X. H., He, J. S., Cao, D., Yu, X. D., Wang, D. D., Burch, J. L., Pollock, C. J., and Torbert, R. B.: Observations of the Electron Jet Generated by Secondary Reconnection in the Terrestrial Magnetotail, The Astrophysical Journal, 862, 144, https://doi.org/10.3847/1538-4357/aacd4c, 2018.

Huang, Z., Tóth, G., van der Holst, B., Chen, Y., and Gombosi, T.: A six-moment multi-fluid plasma model, Journal of Computational Physics, 387, 134–153, https://doi.org/10.1016/j.jcp.2019.02.023, 2019.

Janhunen, P., Palmroth, M., Laitinen, T., Honkonen, I., Juusola, L., Facsko, G., and Pulkkinen, T.: The GUMICS-4 global MHD magnetosphere-ionosphere coupling simulation, Journal of Atmospheric and Solar - Terrestrial Physics, 80, 48–59, https://doi.org/10.1016/j.jastp.2012.03.006, 2012.

Juusola, L., Hoilijoki, S., Pfau-Kempf, Y., Ganse, U., Jarvinen, R., Battarbee, M., Kilpua, E., Turc, L., and Palmroth, M.: Fast plasma sheet flows and X line motion in the Earth's magnetotail: results from a global hybrid-Vlasov simulation, Annales Geophysicae, 36, 1183–1199, https://doi.org/10.5194/angeo-36-1183-2018, 2018a.

Juusola, L., Pfau-Kempf, Y., Ganse, U., Battarbee, M., Brito, T., Grandin, M., Turc, L., and Palmroth, M.: A possible source mechanism for magnetotail current sheet flapping, Annales Geophysicae, 36, 1027–1035, https://doi.org/10.5194/angeo-36-1027-2018, 2018b.

Karimabadi, H., Roytershteyn, V., Vu, H. X., Omelchenko, Y. A., Scudder, J., Daughton, W., Dimmock, A., Nykyri, K., Wan, M., Sibeck, D., Tatineni, M., Majumdar, A., Loring, B., and Geveci, B.: The link between shocks, turbulence, and magnetic reconnection in collisionless plasmas, Physics of Plasmas, 21, 062 308, https://doi.org/10.1063/1.4882875, 2014.

https://doi.org/10.5194/angeo-2020-31
Preprint. Discussion started: 2 June 2020

Kempf, Y., Pokhotelov, D., Von Alfthan, S., Vaivads, A., Palmroth, M., and Koskinen, H. E. J.: Wave dispersion in the hybrid-Vlasov model: Verification of Vlasiator, Physics of Plasmas, 20, 1–9, https://doi.org/10.1063/1.4835315, 2013.

Kilian, P., Muñoz, P. A., Schreiner, C., and Spanier, F.: Plasma waves as a benchmark problem, Journal of Plasma Physics, 83, https://doi.org/DOI: 10.1017/S0022377817000149, 2017.

Lapenta, G., Markidis, S., Marocchino, A., and Kaniadakis, G.: Relaxation of Relativistic Plasmas Under the Effect of Wave-Particle Interactions, The Astrophysical Journal, 666, 949–954, https://doi.org/10.1086/520326, 2007.

Lapenta, G., Markidis, S., Divin, A., Goldman, M., and Newman, D.: Scales of guide field reconnection at the hydrogen mass ratio, Physics of Plasmas, 17, 082 106, https://doi.org/10.1063/1.3467503, 2010.

Lapenta, G., Markidis, S., Goldman, M. V., and Newman, D. L.: Secondary reconnection sites in reconnection-generated flux ropes and reconnection fronts, Nature Physics, 11, 690–695, https://doi.org/10.1038/nphys340, 2015.

Li, W. Y., Graham, D. B., Khotyaintsev, Y. V., Vaivads, A., André, M., Min, K., Liu, K., Tang, B. B., Wang, C., Fujimoto, K., Norgren, C., Toledo-Redondo, S., Lindqvist, P.-A., Ergun, R. E., Torbert, R. B., Rager, A. C., Dorelli, J. C., Gershman, D. J., Giles, B. L., Lavraud, B., Plaschke, F., Magnes, W., Contel, O. L., Russell, C. T., and Burch, J. L.: Electron Bernstein waves driven by electron crescents near the electron diffusion region, Nature Communications, 11, 1–10, https://doi.org/10.1038/s41467-019-13920-w, 2020.

Lin, Y. and Wang, X. Y.: Three-dimensional global hybrid simulation of dayside dynamics associated with the quasi-parallel bow shock, Journal of Geophysical Research, 110, A12 216, https://doi.org/10.1029/2005JA011243, 2005.

Liu, Y.-H. H., Daughton, W., Karimabadi, H., Li, H., and Roytershteyn, V.: Bifurcated Structure of the Electron Diffusion Region in Three-Dimensional Magnetic Reconnection, Physical Review Letters, 110, 265 004, https://doi.org/10.1103/PhysRevLett.110.265004, 2013.

Londrillo, P. and Del Zanna, L.: On the divergence-free condition in Godunov-type schemes for ideal magnetohydrodynamics: the upwind constrained transport method, Journal of Computational Physics, 195, 17–48, https://doi.org/10.1016/j.jcp.2003.09.016, 2004.

Nunn, D.: Vlasov Hybrid Simulation—An Efficient and Stable Algorithm for the Numerical Simulation of Collision-Free Plasma, Transport Theory and Statistical Physics, 34, 151–171, https://doi.org/10.1080/00411450500255518, 2005.

Omidi, N., Phan, T., and Sibeck, D. G.: Hybrid simulations of magnetic reconnection initiated in the magnetosheath, Journal of Geophysical Research: Space Physics, 114, https://doi.org/10.1029/2008JA013647, 2009.

Onsager, T. G., Thomsen, M. F., Elphic, R. C., and Gosling, J. T.: Model of electron and ion distributions in the plasma sheet boundary layer, Journal of Geophysical Research: Space Physics, 96, 20 999–21 011, https://doi.org/10.1029/91JA01983, 1991.

Onsager, T. G., Thomsen, M. F., Elphic, R. C., Gosling, J. T., Anderson, R. R., and Kettmann, G.: Electron generation of electrostatic waves in the plasma sheet boundary layer, Journal of Geophysical Research: Space Physics, 98, 15 509–15 519, https://doi.org/10.1029/93JA00921, 1993.

Palmroth, M.: Vlasiator, Web site, http://www.physics.helsinki.fi/vlasiator/, 2020.

Palmroth, M. and the Vlasiator team: Vlasiator: hybrid-Vlasov simulation code, Github repository, https://doi.org/10.5281/zenodo.3640593, 2020.

Palmroth, M., Hoilijoki, S., Juusola, L., Pulkkinen, T., Hietala, H., Pfau-Kempf, Y., Ganse, U., von Alfthan, S., Vainio, R., and Hesse, M.: Tail reconnection in the global magnetospheric context: Vlasiator first results, Annales Geophysicae, 35, 1269–1274, https://doi.org/10.5194/angeo-35-1269-2017, 2017.

Palmroth, M., Ganse, U., Pfau-Kempf, Y., Battarbee, M., Turc, L., Brito, T., Grandin, M., Hoilijoki, S., Sandroos, A., and von Alfthan, S.: Vlasov methods in space physics and astrophysics, Living Reviews in Computational Astrophysics, 4, 1, https://doi.org/10.1007/s41115-018-0003-2, 2018.

https://doi.org/10.5194/angeo-2020-31
Preprint. Discussion started: 2 June 2020

Palmroth, M., Ganse, U., Pfau-Kempf, Y., Battarbee, M., Turc, L., Brito, T., Grandin, M., Hoilijoki, S., Sandroos, A., and von Alfthan, S.: Vlasov methods in space physics and astrophysics, Living Reviews in Computational Astrophysics, 4, 1, https://doi.org/10.1007/s41115-018-0003-2, 2018.

Paterson, W. R. and Frank, L. A.: Survey of plasma parameters in Earth's distant magnetotail with the Geotail spacecraft, Geophysical Research Letters, 21, 2971–2974, https://doi.org/10.1029/94GL02105, 1994.

Pezzi, O., Cozzani, G., Califano, F., Valentini, F., Guarrasi, M., Camporeale, E., Brunetti, G., Retinò, A., and Veltri, P.: ViDA: a Vlasov–DArwin solver for plasma physics at electron scales, Journal of Plasma Physics, 85, 905850 506, https://doi.org/10.1017/S0022377819000631, 2019.

Phan, T. D., Eastwood, J. P., Shay, M. A., Drake, J. F., Sonnerup, B. U. Ö., Fujimoto, M., Cassak, P. A., Øieroset, M., Burch, J. L., Torbert, R. B., Rager, A. C., Dorelli, J. C., Gershman, D. J., Pollock, C., Pyakurel, P. S., Haggerty, C. C., Khotyaintsev, Y., Lavraud, B., Saito, Y., Oka, M., Ergun, R. E., Retino, A., Le Contel, O., Argall, M. R., Giles, B. L., Moore, T. E., Wilder, F. D., Strangeway, R. J., Russell, C. T., Lindqvist, P. A., and Magnes, W.: Electron magnetic reconnection without ion coupling in Earth's turbulent magnetosheath, Nature, 557, 202–206, https://doi.org/10.1038/s41586-018-0091-5, 2018.

Pritchett, P.: Particle-in-cell simulations of magnetosphere electrodynamics, IEEE Transactions on Plasma Science, 28, 1976–1990, https://doi.org/10.1109/27.902226, 2000.

Ricci, P., Lapenta, G., and Brackbill, J. U.: GEM reconnection challenge: Implicit kinetic simulations with the physical mass ratio, Geophysical Research Letters, 29, 3–1–3–4, https://doi.org/10.1029/2002GL015314, 2002.

Sandroos, A.: VLSV: file format and tools, Github repository, https://github.com/fmihpc/vlsv/, 2019.

Schmitz, H. and Grauer, R.: Kinetic Vlasov simulations of collisionless magnetic reconnection, Physics of Plasmas, 13, 092 309, https://doi.org/10.1063/1.2347101, 2006.

Sibeck, D. G., Omidi, N., Dandouras, I., and Lucek, E.: On the edge of the foreshock: model-data comparisons, Annales Geophysicae, 26, 1539–1544, https://doi.org/10.5194/angeo-26-1539-2008, 2008.

Tóth, G., Jia, X., Markidis, S., Peng, I. B., Chen, Y., Daldorff, L. K. S., Tenishev, V. M., Borovikov, D., Haiducek, J. D., Gombosi, T. I., Glocer, A., and Dorelli, J. C.: Extended magnetohydrodynamics with embedded particle-in-cell simulation of Ganymede's magnetosphere, Journal of Geophysical Research: Space Physics, 121, 1273–1293, https://doi.org/10.1002/2015JA021997, 2016.

Tóth, G., Chen, Y., Gombosi, T. I., Cassak, P., Markidis, S., and Peng, I. B.: Scaling the Ion Inertial Length and Its Implications for Modeling Reconnection in Global Simulations, Journal of Geophysical Research: Space Physics, 122, 10,336–10,355, https://doi.org/10.1002/2017JA024189, 2017.

Umeda, T., Togano, K., and Ogino, T.: Two-dimensional full-electromagnetic Vlasov code with conservative scheme and its application to magnetic reconnection, Computer Physics Communications, 180, 365 – 374, https://doi.org/https://doi.org/10.1016/j.cpc.2008.11.001, 2009.

von Alfthan, S., Pokhotelov, D., Kempf, Y., Hoilijoki, S., Honkonen, I., Sandroos, A., and Palmroth, M.: Vlasiator: First global hybrid-Vlasov simulations of Earth's foreshock and magnetosheath, Journal of Atmospheric and Solar-Terrestrial Physics, 120, 24–35, https://doi.org/10.1016/j.jastp.2014.08.012, 2014.

Wang, C.-P., Gkioulidou, M., Lyons, L. R., and Angelopoulos, V.: Spatial distributions of the ion to electron temperature ratio in the magnetosheath and plasma sheet, Journal of Geophysical Research (Space Physics), 117, A08 215, https://doi.org/10.1029/2012JA017658, 2012.

https://doi.org/10.5194/angeo-2020-31
Preprint. Discussion started: 2 June 2020

565 Wang, J., Huang, C., Ge, Y. S., Du, A., and Feng, X.: Influence of the IMF Bx on the geometry of the bow shock and magnetopause, Planetary and Space Science, 182, 104 844, https://doi.org/https://doi.org/10.1016/j.pss.2020.104844, 2020.

Wilson, F., Neukirch, T., Hesse, M., Harrison, M. G., and Stark, C. R.: Particle-in-cell simulations of collisionless magnetic reconnection with a non-uniform guide field, Physics of Plasmas, 23, 032 302, https://doi.org/10.1063/1.4942939, 2016.

Yamamoto, T. and Tamao, T.: Adiabatic plasma convection in the tail plasma sheet, Planetary and Space Science, 26, 1185 – 1191,
570 https://doi.org/https://doi.org/10.1016/0032-0633(78)90058-2, 1978.

Zerroukat, M. and Allen, T.: A three-dimensional monotone and conservative semi- Lagrangian scheme (SLICE-3D) for transport problems, Quarterly Journal of the Royal Meteorological Society, 138, 1640–1651, https://doi.org/10.1002/qj.1902, 2012.

Zhou, H., Tóth, G., Jia, X., Chen, Y., and Markidis, S.: Embedded Kinetic Simulation of Ganymede's Magnetosphere: Improvements and Inferences, Journal of Geophysical Research: Space Physics, 124, 5441–5460, https://doi.org/10.1029/2019JA026643, 2019.